Mine Water Environ (2018) 37:119–136
DOI 10.1007/s10230-017-0477-x

TECHNICAL ARTICLE

Hydrochemical and Stable Isotope (δD and $\delta^{18}O$) Characteristics of Groundwater and Hydrogeochemical Processes in the Ningtiaota Coalfield, Northwest China

Xujuan Huang[1,2] · Guangcai Wang[1,2] · Xiangyang Liang[1,3] · Linfeng Cui[1,4] · Luan Ma[1] · Qingyu Xu[1]

Received: 6 August 2016 / Accepted: 24 July 2017 / Published online: 31 July 2017

Abstract Understanding the sources and mechanisms of groundwater recharge in the Ningtiaota Coalfield, an arid area in northwest China, is important for water resources management and coal mine safety. Hydrochemical and stable hydrogen and oxygen isotopic data were used to study water–rock interactions and groundwater recharge in the area. A total of 45 water samples, including surface water, Quaternary groundwater, and Jurassic Zhiluo Group (J_2z) and Yan'an Group (J_2y) groundwater, were collected for major ions and stable isotope (δD and $\delta^{18}O$) analyses. Our results showed that the groundwater originated from atmospheric precipitation, and experienced weak evaporation during infiltration. Water in the study area has a low salinity and is dominated by HCO_3–Ca type. The dominant water–rock interactions in the Jurassic Zhiluo Group (J_2z) groundwater were dissolution of silicate minerals, gypsum, and halite and cation exchange. The results may aid in water resources management and groundwater inrush prevention in the coalfield and at other coal mines.

Keywords Arid and semi-arid areas · Hydrogeochemical evolution · Water–rock interaction

✉ Guangcai Wang
wanggc@pku.edu.cn

[1] State Key Laboratory of Biogeology and Environmental Geology and MOE Key Laboratory of Groundwater Circulation and Environment Evolution, China University of Geosciences, Beijing 100083, China

[2] School of Water Resources and Environment, China University of Geosciences, Beijing 100083, China

[3] CCTEG Xi'an Research Institute, Xi'an 710054, China

[4] China Institute of Geo-environment Monitoring, Beijing 100081, China

Introduction

With the revival of the Silk Road economic belt (Li et al. 2015), groundwater will become even more important for western China, and research on groundwater quality will be more urgent and important for the sustainable development of western China (Li 2016). The Ningtiaota Coalfield of northern Shaanxi, one of the main coal mining areas in northwest China, has abundant and high-quality Jurassic coal resources (Wang et al. 2009). Over the last few decades, with the increasing exploitation of underground coal reserves, groundwater inrush has become a severe threat to mine safety in the northern Shaanxi region. To prevent groundwater inflows into coal mines, groundwater is constantly pumped to reduce the water pressure, which has undoubtedly caused a waste of groundwater resources in the region where groundwater is the main source of water supply (Li et al. 2013a). In addition, long-time depressurization and dewatering may change the flow systems and the quality of groundwater and surface water (Hu and Evans 1997; Jiang et al. 2010; Zhang and Liu 2002). Therefore, it is very important to understand groundwater circulation and groundwater quality/hydrochemical processes.

The hydrochemical method is one of the most common and effective approaches to identify groundwater circulation. Along the general groundwater flow direction, the ions' concentrations change because of water–rock interactions between groundwater and aquifer materials. The chemical composition of groundwater is controlled by the composition and quantity of rainfall, the geological structure, the aquifer minerals, and hydrochemical evolution processes along flow paths (André et al. 2005; Gastmans et al. 2010; Moral et al. 2008). Therefore, spatial variations in the chemistry of groundwater can be useful in elucidating the groundwater's origin, circulation, and

water–rock interactions (Sun et al. 2009; Wang et al. 2006), and can play an important role in discriminating groundwater inrush sources and passages, and hydraulic connections between aquifers (Wang et al. 2000). In combination with other data on geology, hydrology, and isotopes, information on groundwater hydrochemistry can be helpful in understanding the recharge and discharge characteristics of groundwater (Gomo and Vermeulen 2014; Han et al. 2013; Murkute 2014). In recent years, hydrochemistry and isotope approaches have become an integral part of study on groundwater circulation (Chen et al. 2013; Clark and Fritz 1997; Huang and Chen 2012; Kendall and McDonnell 1998; Wang et al. 2013).

A series of geological, geophysical, and hydrogeological studies have been conducted to understand the lithology, coal distribution, and hydrogeological conditions of the Ningtiaota Coalfield (Xi'an Research Institute 2012; Shaanxi Coalfield Geology Bureau 1987). More attention has been paid to groundwater behavior due to the increasing competition between groundwater consumption and mine safety. This study reports on the chemical and isotopic composition of groundwater from three main aquifers. The data were used to assess groundwater quality and identify the hydraulic connectivity between the aquifers before mining began.

Study Area

The Ningtiaota Coalfield is located in the northwest of Shenmu County, Yulin City of Shaanxi Province, China, and is approximately 36 km from Shenmu County. The coalfield covers an area of 71.20 km^2 (Fig. 1; Yao and Xia 2007). The study area is located in the warm temperate zone with an average annual temperature of 8.6 °C, and is characterized by a semi-arid continental monsoon climate. According to observational data from 1961 to 2003 at the Shenmu weather station, the mean annual precipitation is 434.1 mm, and the mean annual evaporation is 1712.0 mm (Su et al. 2013). The rainy season (July–September) typically accounts for 50–70% of the total year's rainfall.

The elevation of the study area is higher in the southwest than in the northeast. The overall topography is relatively flat with the highest elevation (1328 m) in Gongjialiang and the lowest (1121 m) in the downstream Kaokaowusu River, near the area's eastern boundary. The Ningtiaota Coalfield is located in the Kuye River basin, which belongs to the Yellow River. The rivers in the area are mainly the Kaokaowusu (KKWS) River and its tributaries, the Kentieling (KTL), Dahoujiamu (DHJM), and Xiaohoujiamu (XHJM) Rivers, and the Majiata River's branch Lucao (LCG) River, which is near the study area's southern boundary (Fig. 1). There are two landforms in the area: a sandy area, which is widely distributed and accounts for about 90% of the total area, and the river valleys in the basins of the Kaokaowusu (KKWS) River and its tributaries (Figs. 1, 2).

Geology and Hydrogeology

The Ningtiaota Coalfield is located in the northeast of the Ordos Basin (Fig. 1), which developed during the Mesozoic Era on the North China craton. The interior of the basin was relatively stable although the margins were tectonically active (Wang et al. 2014; Xue et al. 2010). The study area was in the interior of the basin and mainly went through vertical lifting and depression without magmatic activity or large faults. The regional strata incline to the northwest, forming monoclinic structures with an inclination of 1° (Ding et al. 2016; Xue et al. 2010; Yang et al. 2015a). The strata sequences from top to bottom are the Quaternary Holocene alluvium (Q_4^{al}) and eolian sand (Q_4^{eol}), the Middle Pleistocene Lishi Group (Q_2l), the Neogene Pliocene Baode Group (N_2b), the Middle Jurassic Zhiluo Group (J_2z), and the Yan'an Group (J_2y) (Li et al. 2013a, 2008; Yang et al. 2015b). Each stratum (except the Quaternary) contacts conformably or para-unconformably. The main mining coal seam (2^{-2}) is located in the Yan'an Group (J_2y). The floor of the coal seam gently undulates.

The main top–down aquifers are the Quaternary Holocene alluvium (Q_4^{al}) aquifer, the Upper Pleistocene Salawusu Group (Q_3s) alluvial aquifers, the Jurassic Zhiluo Group (J_2z) weathered, fractured aquifer, the Jurassic Yan'an Group (J_2y) sandstone aquifer. The aquicludes includes the Lishi Group (Q_2l) loess aquiclude and the Baode Group (N_2b) laterite aquiclude (Fig. 2) (Xi'an Research Institute 2012). Among them, the Jurassic Zhiluo Group (J_2z) weathered, fractured aquifer, which overlies the coal-bearing strata Yan'an Group, is one of most important aquifers, as groundwater in the Zhiluo Group aquifer is both used as a main source for water supply and is a potential threat to coal mining in the Ningtiaota Coalfield. The aquifer is characterized as medium-coarse-grained gravel-bearing feldspar sandstone with well-developed weathered fractures. Its thickness ranges from 10.00 to 33.76 m. It is recharged by groundwater from the lateral or overlying aquifer through weathered fractures. On the basis of pumping and draining tests conducted in the coalfield, the hydraulic conductivity and specific capacity of the aquifer is 1.98–28.80 m/day and 0.019–0.032 L s m, respectively, indicating high permeability and weak water yield. The thickness of the Jurassic Yan'an Group (J_2y) sandstone aquifer ranges from 21.75 to 114.13 m, the hydraulic conductivity and specific capacity is 2.69×10^{-4}–3.00×10^{-4} m/day and 6.52×10^{-5}–5.80×10^{-4} L/s m, respectively, indicating poor permeability and poor water yield. The hydraulic

connection between the Quaternary and Jurassic aquifers is weak, as demonstrated by the drainage tests (Xi'an Research Institute 2012). The water levels in the three boreholes (J12, J17, SYJ) in the Jurassic aquifer decreased soon after the Zhiluo group groundwater drained, while there was no distinct change in the water level in the Q5 borehole (Fig. 3).

Groundwater flow in the study area is mainly controlled by topography and bounded by the watershed (approximately from Shinibula to Gongjialiang, Fig. 2). Groundwater in the north of the watershed flows towards the northeast and then discharges to the Kaokaowusu (KKWS) River, while groundwater in the south flows to the southeast and eventually discharges to the Lucao (LCG) River (Fig. 2). In recent years, mine drainage pumped from the underground mine has become another important source of groundwater discharge apart from natural discharge (Xi'an Research Institute 2012; Jiang et al. 2010).

Samples Collection and Analysis

Forty-five water samples, including 9 surface water, 4 Quaternary groundwater, 24 Zhiluo Group (J_2z,) and 8 Yan'an Group (J_2y) groundwater samples were collected in the study area (Fig. 2). The groundwater samples were collected with bailers. Most of the samples were collected in both March and August, 2012. Some samples were collected again in August 2013. The hydrochemical composition of the samples suggests minor temporal variations.

Immediately after collection, all samples were filtered through 0.45 μm membrane filters. Aliquots of the water

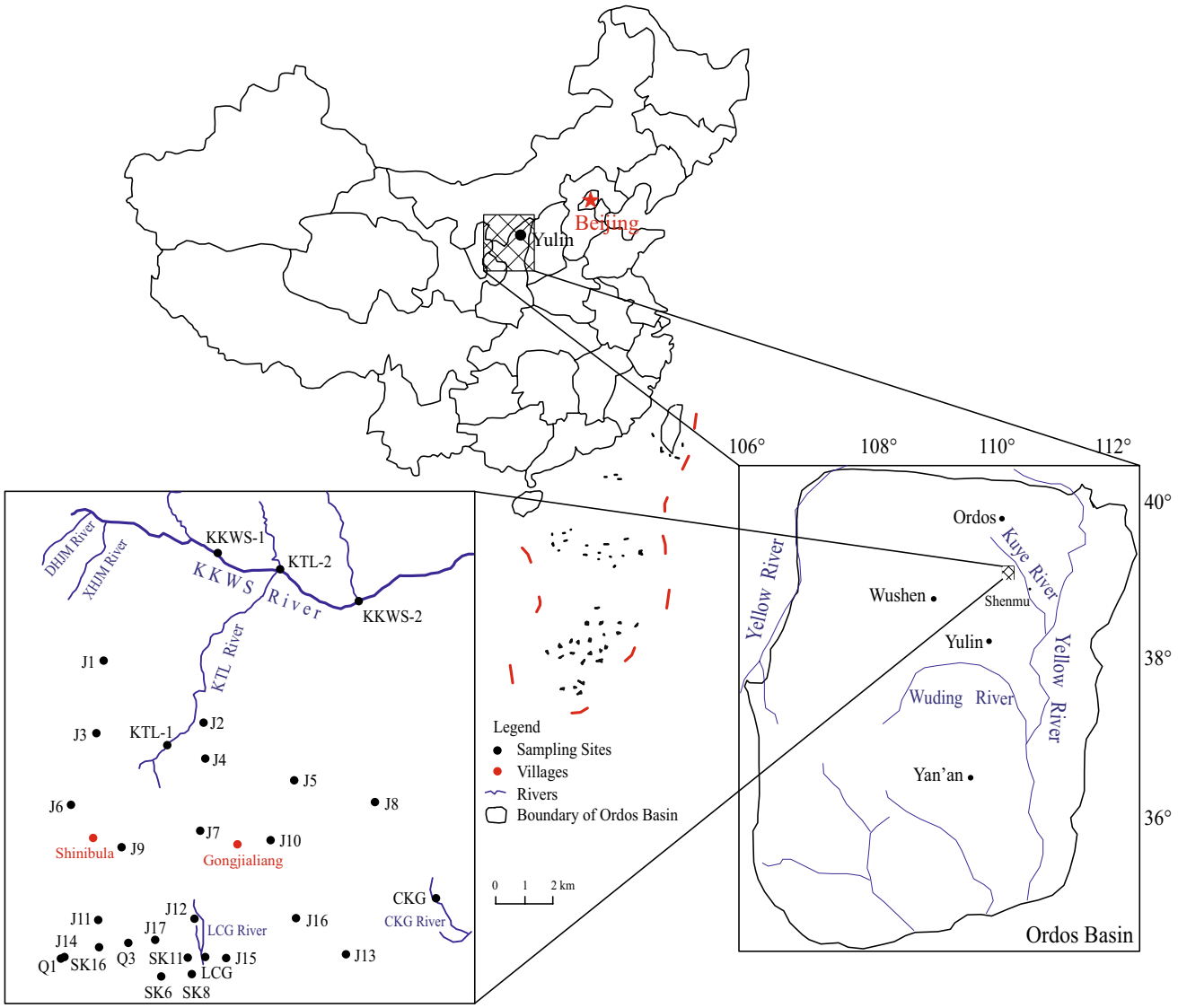

Fig. 1 Geographical location of the study area

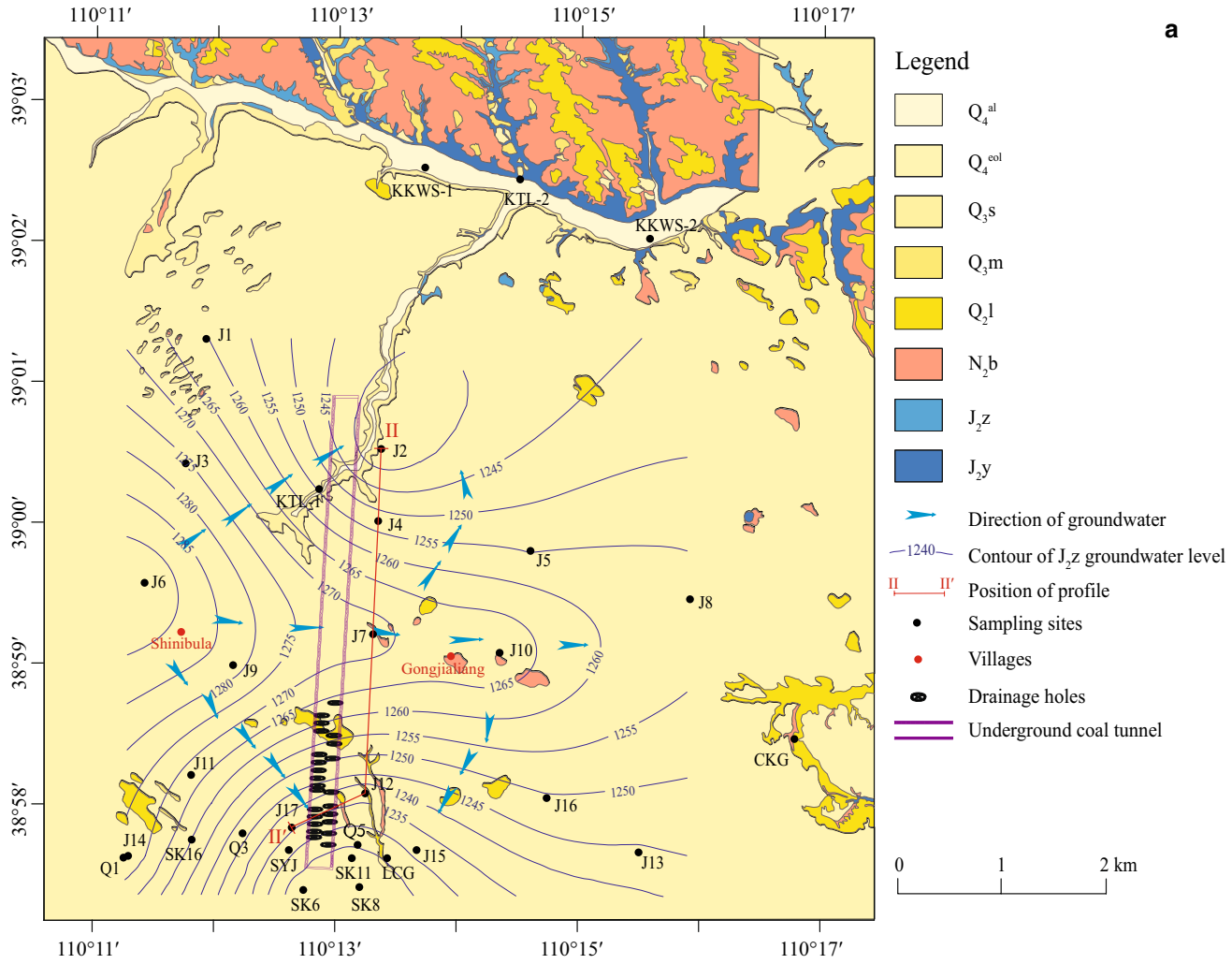

Fig. 2 Sketch map of hydrogeology of the study area (after Xi'an Research Institute 2012): **a** hydrogeological sketch of the study area and the distribution of water samples, **b** hydrogeological profile of II–II′

were stored for anion and stable hydrogen and oxygen isotope analyses. The aliquots for cation analyses were acidified to pH < 2 with ultra-purified nitric acid and stored in polyethylene bottles. Four parameters were measured in the field (DO, ORP, electrical conductivity (EC), and pH) with portable multi-parameter instruments (DO30 dissolved oxygen (DO), ORP30 ORP, CON30 EC, and pH30 pH probes, respectively). Major cations (Ca, Mg, Na, K) were measured with a Spectroblue inductively coupled plasma optical emission spectrometer (ICP-OES), anions (SO_4, Cl, NO_3, and F) were measured by DX-120 IC (ion chromatography), and the alkalinity was titrated using a HCl standard solution (0.025 mol/L). The total dissolved solids (TDS) were calculated as the sum of major ion concentrations, subtracting a half of the HCO_3. The precision of cations and anions (except for HCO_3 and CO_3) is 0.01 mg/L; the precision of HCO_3 and CO_3 is 0.6 mg/L. Stable isotopes (δD, $\delta^{18}O$) were determined by isotope ratios using LGR LWIA-24d (liquid–water isotope analyzer) and reported relative to the VSMOW standard (Vienna Standard Mean Ocean Water) in permil (‰); the precision is 0.03‰ for δD and 0.28‰ for $\delta^{18}O$, respectively. Hydrochemical and stable isotope compositions are presented in Table 1.

Results and Discussion

A regional hydrogeochemical study is intrinsically a multivariate problem because of the diverse parameters (variables) associated with a large number of sampling sites (observations). Although multivariate statistical methods do not indicate cause-and-effect relationships, they provide information from which such relationships can be inferred (Monjerezi et al. 2011). Therefore, they have been used extensively in analysis of hydrogeochemical data and have contributed to the discovery of major mechanisms

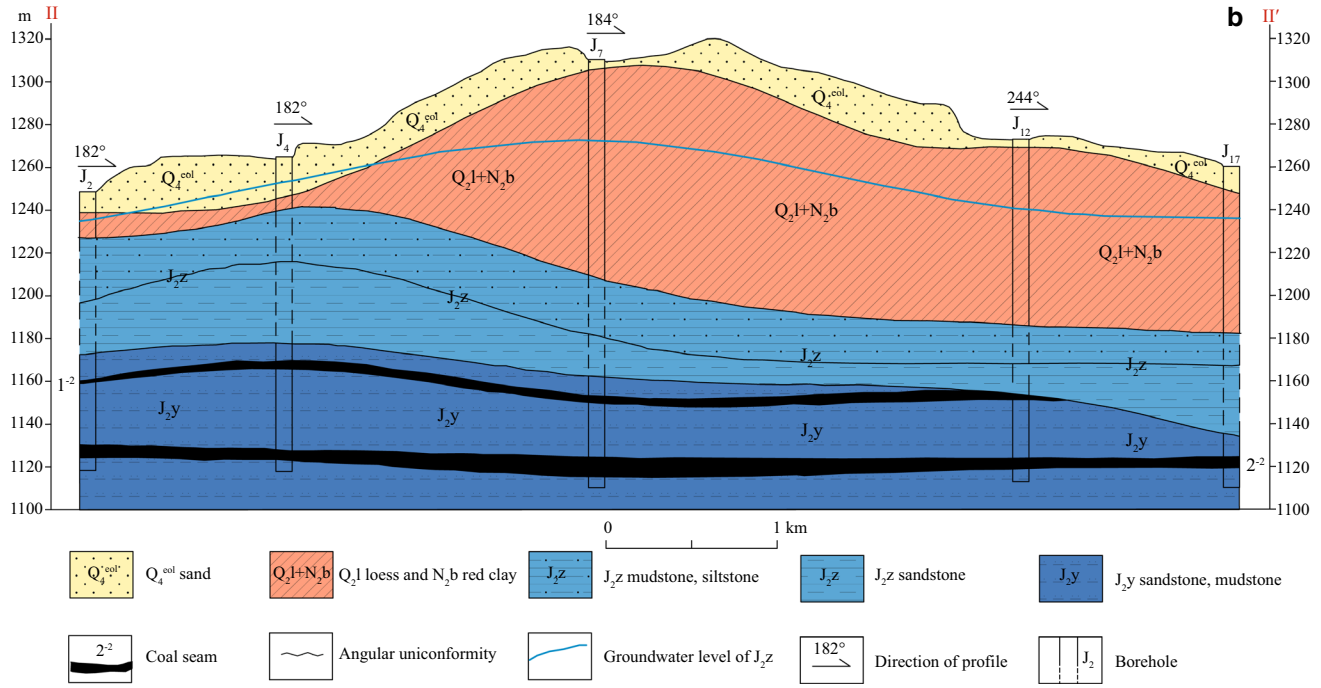

Fig. 2 (continued)

influencing groundwater chemistry. In this study, we used descriptive statistical analysis and a set of graphical representations to explore the hydrogeochemical characteristics, ion sources, and associated hydrogeochemical processes.

Hydrogeochemical Characteristics

Descriptive statistical analyses (minimum, maximum, and mean) of the data are shown in Table 2 and are plotted as box-plots (Fig. 4). All of the samples had low salinity (TDS < 500 mg/L). The Quaternary water had a high NO_3 content (averaging 26.52 mg/L), which might be due to agricultural activities given how close the unconfined aquifer is to human activities. Sample J7 (belonging to J_2z) had detectable CO_3^{2-}, while the other samples did not. The Ca, Mg, and TDS content of the Zhiluo and Yan'an Groups were generally less than that of the surface water and Quaternary groundwater; and four outliers (J11, J10, J15, and J13) had relatively high SO_4 concentrations. According to the GB/T 14848-1993 Quality Standard for Ground Water (Ministry of Land and Resources of the People's Republic of China 1993), the groundwater quality was classified into five types on the basis of 39 indicators, including NO_3. In terms of NO_3 concentration, all samples except for the Quaternary Q1 (65.5 mg/L) were better than type II ($NO_3 \leq 22$ mg/L), indicating that the natural background groundwater chemical contents were suitable for all purposes.

A Piper diagram (Piper 1944) of J_2z groundwater (Fig. 5) and percentage histograms of the other samples (Fig. 6) are plotted to represent the relative major ion content. They identify the main hydrochemical facies of the different water bodies: surface water is HCO_3–Ca type, Quaternary groundwater is HCO_3–Ca and HCO_3–Ca–Mg types, J_2z groundwater is HCO_3–Ca, HCO_3–Ca–Na + K–Mg, and HCO_3–SO_4–Ca–Na–Mg types, and J_2y groundwater is HCO_3–Ca and HCO_3–Na + K–Ca–Mg types. The dominant hydrochemical type is HCO_3–Ca.

Piper diagrams graphically represent the relative content of major ions in water samples and is widely used to evaluate hydrochemical evolution of surface water and groundwater (Subrahmanyam and Yadaiah 2001). The hydrochemical evolution of the J_2z groundwater can be seen in Fig. 5. In general, the samples in the diamond mostly fall in area 5, which means that carbonate hardness exceeds 50%, i.e. the relative Ca + Mg and $HCO_3 + CO_3$ content exceed 50% of the total cation and anion contents, respectively. With respect to anions, all of the water samples plotted in zone E (HCO_3 type). HCO_3 was the dominant cation, accounting for 60–90%, SO_4 was second with a content of 1–30%, whereas Cl was less than 10%. With respect to cations, samples mostly plotted in zone A (Ca type) and zone B (no dominant type), with significant cationic changes. Ca was the dominant cation accounting for 25–70%, Mg was second (20–40%), and Na + K was least (10–40%).

There are two different evolution patterns regarding the spatial hydrochemical distributions of the J_2z

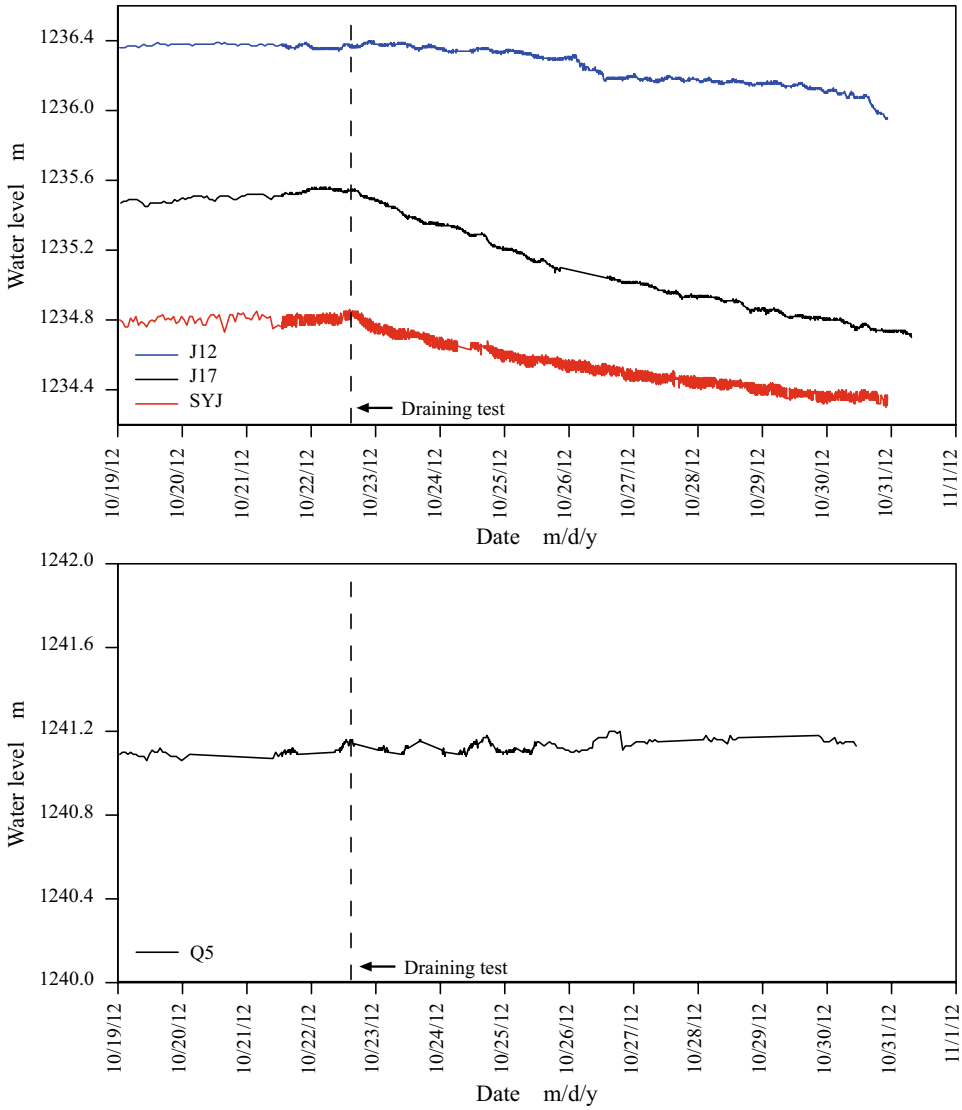

Fig. 3 Water level changes with time in three boreholes

groundwater (Fig. 5). The first pattern (Arrow I) shows the hydrochemical changes, from HCO_3–Na + K–Ca–Mg to HCO_3–Ca, with an obvious increase in TDS (Table 1) along the groundwater flow direction (such as from J9 to J12, Fig. 2a). The essence of the changes is an increase in Ca (from 9.61 to 47.15 mg/L) and HCO_3 (from 74.55 to 181.97 mg/L), while the concentrations of the other ions remained relatively constant. This was likely due to hydrolysis of calcium silicates (Eq. 1).

Another evolution pattern represents the changes of hydrochemical type from HCO_3–Na + K–Ca–Mg to $HCO_3(CO_3)$–Na + K, without an obvious change in TDS (Table 1) from J9 to J7 (Arrow II). The essence of the changes is an increase in Na (from 10.47 to 18.82 mg/L), K (from 1.43 to 16.16 mg/L) and CO_3 (from undetected to 21.34 mg/L), while Ca (from 9.61 to 2.51 mg/L), Mg (from 4.63 to 0.16 mg/L) and HCO_3 (from 74.55 to 32.82 mg/L) decreased. The main water–rock interaction of the second pattern was likely due to dissolution of aluminosilicate minerals accompanied by the precipitation of calcite/dolomite (Eq. 2; Shvartsev and Wang 2006) or cation exchange (Eq. 3). During the cation exchange process, 1 mmol/L Ca in the water will be changed to 2 mmol/L Na; this process does not change the TDS significantly because the weight of 1 mmol/L Ca (40 mg/L) is approximately equal to 2 mmol/L Na (46 mg/L).

$$CaAl_2Si_2O_8 + 4CO_2 + 6H_2O = 2Al_2Si_2O_5(OH)_4 + 2Ca^{2+} + 4HCO_3^- \quad (1)$$

$$CaAl_2Si_2O_8 \cdot 2NaAlSi_3O_8 + 3CO_2 + 5H_2O = 2Al_2Si_2O_5(OH)_4 + CaCO_3 + 4SiO_2 + 2Na^+ + 2HCO_3^- \quad (2)$$

$$2Na^+/K^+(clay) + Ca^{2+}/Mg^{2+}(water) = 2Na^+/K^+(water) + Ca^{2+}/Mg^{2+}(clay). \quad (3)$$

Table 1 Hydrochemical results and isotope compositions of the study area

Sample	Ca	Mg	Na	K	HCO_3	SO_4	Cl	CO_3	NO_3	Fe	pH	E (%)	TDS	Hard	δD	$\delta^{18}O$	SI_{cal}	SI_{dol}	SI_{gyp}
LCG-1																			
SW	55.49	8.47	9.21	0.79	224.23	11.45	5.46	nd	9.38	nd	8.40	−4.05	212.66	174.02	−65.72	-8.82	1.03	1.26	−2.57
LCG-2																			
SW	54.63	8.33	9.17	0.79	211.31	11.86	5.67	nd	9.22	nd	–	−2.35	205.62	171.28	-64.29	−8.49	–	–	–
KTL-1																			
SW	51.59	7.66	7.83	0.55	198.96	13.91	5.17	nd	6.75	nd	8.04	−3.30	193.25	160.89	-67.38	−9.10	0.61	0.69	−2.51
KTL-2																			
SW	54.96	8.45	8.85	0.85	207.68	17.97	5.83	nd	8.64	nd	–	−2.89	209.64	172.61	−65.26	−8.85	–	–	–
KKWS-1																			
SW	55.38	11.08	16.65	1.36	215.37	30.86	7.12	nd	7.48	nd	8.61	−0.56	237.99	184.62	−67.01	−8.99	1.00	1.59	−2.17
KKWS-2																			
SW	58.16	10.85	13.51	1.56	233.82	20.21	7.92	nd	7.19	nd	–	−1.87	236.77	190.61	−64.40	−8.54	–	–	–
KKWS-3																			
SW	54.08	10.72	14.91	1.45	214.94	27.07	7.63	nd	7.84	nd	–	−1.74	231.50	179.87	−66.34	−8.77	–	–	–
CKG																			
SW	56.89	8.84	9.23	0.84	216.38	12.89	5.61	nd	9.93	nd	–	−1.70	212.69	179.06	−64.76	−8.58	–	–	–
CJG																			
SW	50.89	9.59	11.87	1.34	206.22	15.39	9.44	nd	6.33	nd	–	−2.31	208.26	167.18	−61.83	−8.00	–	–	–
Q1-1																			
Q_4^{eol} GW	90.20	7.90	14.20	0.70	210.50	48.00	12.40	nd	65.50	0.10	7.90	−0.32	344.47	258.42	–	–	0.68	0.60	−1.83
Q1-2																			
Q_4^{eol} GW	77.53	6.96	10.25	0.52	208.25	46.06	6.52	nd	39.35	nd	–	−2.65	291.50	222.83	−65.04	−8.78	–	–	–
Q3-1																			
Q_4^{eol} GW	18.26	7.41	10.54	2.07	117.05	7.76	5.70	nd	0.27	nd	–	−5.01	110.83	76.53	−68.76	−9.06	–	–	–
Q3-2																			
Q_4^{eol} GW	21.02	8.37	10.37	1.53	133.05	2.71	4.89	nd	0.95	nd	–	−3.55	116.62	87.43	−68.82	−9.24	–	–	–
J1																			
J_2z GW	47.10	8.50	9.90	0.70	183.10	2.40	7.10	nd	19.80	0.20	8.01	−0.95	187.64	153.17	–	–	0.52	0.57	−3.30
J2-1																			
J_2z GW	19.74	5.68	14.85	1.59	118.80	9.59	6.12	nd	0.31	nd	9.20	−4.19	117.54	73.02	−67.10	−8.72	1.05	1.86	−3.03
J2-2																			
J_2z GW	27.37	6.45	7.70	1.09	135.94	5.68	3.08	nd	0.35	nd	–	−3.88	120.00	95.30	−66.53	−8.86	–	–	–
J3																			
J_2z GW	44.10	9.10	11.20	0.80	183.10	7.20	5.30	nd	13.00	0.20	7.97	−0.53	182.60	148.17	–	–	0.45	0.50	−2.85
J4																			
J_2z GW	27.10	14.60	12.90	1.20	137.30	16.80	7.10	3.00	11.80	nd	8.43	1.19	163.26	128.58	–	–	0.56	1.15	−2.68

Table 1 (continued)

Sample	Ca	Mg	Na	K	HCO_3	SO_4	Cl	CO_3	NO_3	Fe	pH	E (%)	TDS	Hard	δD	$\delta^{18}O$	SI_{cal}	SI_{dol}	SI_{gyp}
J5																			
J_2z GW	49.10	12.20	26.70	1.00	204.40	36.00	12.40	nd	16.50	0.30	7.92	−1.34	258.37	173.58	–	–	0.46	0.61	−2.15
J6																			
J_2z GW	38.10	8.50	11.40	0.50	152.60	12.00	5.30	3.00	9.50	0.30	8.55	−0.42	165.20	130.67	–	–	0.86	1.37	−2.68
J7-1																			
J_2z GW	2.51	0.16	18.82	16.16	32.82	8.82	4.75	15.86	nd	nd	10.97	−0.80	83.74	6.94	−73.29	−9.80	0.21	−0.48	−3.88
J7-2																			
J_2z GW	1.68	nd	19.44	14.39	14.46	10.83	3.15	21.34	nd	nd	–	0.76	78.42	4.20	−72.27	−9.50	–	–	–
J8																			
J_2z GW	19.00	9.10	26.60	0.80	164.80	7.20	3.50	nd	nd	nd	8.22	−1.23	148.81	85.42	–	–	0.31	0.58	−3.16
J9-1																			
J_2z GW	12.14	5.06	10.54	1.51	71.45	8.11	5.11	nd	6.57	nd	8.39	−2.36	85.01	51.43	−67.85	−8.72	−0.04	−0.18	−3.24
J9-2																			
J_2z GW	9.61	4.63	10.47	1.43	74.55	8.05	4.94	nd	1.17	nd	–	−6.85	77.84	43.32	−67.25	−8.93	–	–	–
J10																			
J_2z GW	30.10	8.50	28.10	0.80	119.00	50.40	5.30	3.00	7.00	0.10	8.56	1.52	193.06	110.67	–	–	0.48	0.53	−2.16
J11																			
J_2z GW	35.10	15.80	34.13	0.90	177.00	60.00	5.30	nd	11.50	nd	8.23	1.17	251.47	153.58	–	–	0.55	1.05	−2.07
J12-1																			
J_2z GW	47.15	7.26	9.58	1.03	181.97	5.97	3.88	nd	12.62	nd	7.89	−0.43	178.81	148.13	−67.47	−8.84	0.40	0.27	−2.90
J12-2																			
J_2z GW	46.41	7.15	9.74	0.97	181.83	6.04	4.20	nd	13.22	nd	7.84	−1.28	178.96	145.82	−67.78	−8.89	0.34	0.16	−2.90
J13-1																			
J_2z GW	20.00	4.90	53.90	3.00	137.30	36.00	24.80	3.00	0.80	0.70	8.50	0.48	216.33	70.42	–	–	0.36	0.22	−2.47
J13-2																			
J_2z GW	34.10	9.70	6.60	1.00	146.40	7.20	3.50	3.00	1.80	0.10	8.47	0.83	140.41	125.67	−64.89	−8.72	0.74	1.22	−2.93
J14-1																			
J_2z GW	10.29	8.58	13.29	1.93	94.69	7.55	7.18	nd	0.21	nd	9.44	−1.93	96.72	61.48	−69.01	−9.21	0.86	1.94	−3.42
J14-2																			
J_2z GW	8.03	8.23	11.86	1.37	85.32	7.90	7.72	nd	0.00	nd	–	−4.67	88.17	54.37	−72.29	−9.81	–	–	–
J15																			
J_2z GW	22.00	9.70	24.60	0.80	103.70	40.80	7.10	nd	11.50	0.10	8.22	1.27	168.61	95.42	–	–	0.15	0.24	−2.37
J16																			
J_2z GW	44.10	8.50	6.80	0.90	173.90	4.80	5.30	nd	3.80	nd	7.89	0.56	161.86	145.67	–	–	0.36	0.29	−3.01
J17-1																			
J_2z GW	10.98	5.21	10.34	1.66	82.05	9.77	5.52	nd	0.19	nd	9.37	−7.55	84.95	49.16	−64.53	−8.50	0.80	1.57	−3.24

Table 1 (continued)

Sample	Ca	Mg	Na	K	HCO_3	SO_4	Cl	CO_3	NO_3	Fe	pH	E (%)	TDS	Hard	δD	$\delta^{18}O$	SI_{cal}	SI_{dol}	SI_{gyp}
J17-2																			
J_2z GW	12.12	4.74	10.19	1.73	87.57	8.71	5.36	nd	0.14	nd	–	−8.91	87.03	50.05	−63.75	−8.20	–	–	–
SK6-1																			
J_2y GW	7.23	3.14	43.28	3.91	59.54	7.15	5.73	nd	5.34	nd	10.08	−2.48	131.54	31.16	−67.80	−9.00	–	–	–
SK6-2																			
J_2y GW	8.35	5.56	30.59	0.15	71.16	5.02	4.89	nd	4.50	nd	–	−4.58	112.65	44.04	−65.88	−8.80	–	–	–
SK8-1																			
J_2y GW	10.78	4.82	12.26	2.63	86.56	7.04	5.48	nd	0.36	nd	–	−6.10	87.00	47.03	−69.41	−9.28	0.89	1.75	−3.41
SK8-2																			
J_2y GW	9.63	5.30	10.20	1.57	73.03	2.04	5.02	nd	6.50	nd	–	−3.58	77.26	46.16	−67.49	−9.46	–	–	–
SK11-1																			
J_2y GW	9.66	4.10	11.31	2.56	89.17	13.69	18.01	9.72	0.18	nd	9.72	−30.85	114.58	41.23	−67.50	−8.90	–	–	–
SK11-2																			
J_2y GW	9.29	3.70	10.84	0.58	56.20	11.06	17.01	27.00	0.17	nd	–	−34.13	108.41	38.64	−65.67	−8.67	–	–	–
SK16-1																			
J_2y GW	41.67	7.20	12.05	1.54	164.25	13.46	12.93	nd	4.00	nd	7.92	−2.42	175.21	134.18	−64.92	−8.31	0.34	0.20	−2.59
SK16-2																			
J_2y GW	41.22	6.71	11.35	1.44	174.27	13.76	11.34	nd	0.20	nd	–	−4.85	173.37	131.01	−65.39	−8.51	–	–	–

Unit of concentration: mg/L; unit of stable isotopes: ‰ vs VSMOW

The charge balance errors [E (%)] of SK11-1 and SK11-2 are higher than 30%, it is most likely to be affected by tracer NH_4Cl putted in the drilling SK11 during the draining test beginning on February 15, 2012. Seeing from the test results that the concentration of Cl is apparently higher than other samples', and the exclusion of NH_4 in hydrochemical analyses resulted in the negative charge balance error

The concentrations of Na are abnormally high in SK6-1, SK6-2, which should be relevant to the tracer NaF putted in the drilling SK6 during the draining test beginning on 15 February 2012

SK11-1, SK11-2, SK6-1 and SK6-2 were excluded in the subsequent analyses

SW surface water, *Hard* hardness, *GW* groundwater, *cal* calcite, *dol* dolomite, *gyp* gypsum, *nd* concentration below the detection limit, – not tested

The hydrochemistry of the four samples (J13, J10, J11, and J15) circled in zone III (Fig. 5) were HCO_3–SO_4–Ca–Na + K–Mg and HCO_3–Na + K–Ca, with SO_4 concentrations exceeding 20%, which is relatively high. The ratio of Ca to SO_4 in the four samples is close to 1 (Fig. 8f), which suggests that the increased SO_4 was likely due to dissolution of gypsum.

Natural Sources of Ions

Gibbs proposed two diagrams to assess the natural sources of dissolved chemical constituents. The diagrams represent the equivalence ratios of Na/(Na + Ca) and Cl/(Cl + HCO_3) as a function of TDS, which can be used to study how chemical constituents form. The proposed mechanisms in the diagrams include precipitation dominance, rock weathering dominance, and evaporation–crystallization process (Gibbs 1970).

In the Gibbs diagram, samples with low TDS but a high Na/(Na + Ca) or Cl/(Cl + HCO_3) (close to 1) would fall in the lower right, suggesting a significant influence of atmospheric precipitation on the chemical compositions. Samples with medium TDS and medium (around or below 0.5) Na/(Na + Ca) or Cl/(Cl + HCO_3), falling in the middle left, indicate rock weathering dominance. Samples with high TDS and high Na/(Na + Ca) or Cl/(Cl + HCO_3) (close to 1), fall in the upper right, reflecting samples that have experienced intensive evaporation in arid regions.

In the present study, the Gibbs diagrams (Fig. 7) show that chemical weathering of rock-forming minerals is the main process controlling the chemical compositions of groundwater in the study area. The scatter of Na/(Na + Ca) values from low to high without remarkable variations in TDS suggests that cation exchange also influences the chemical compositions by increasing Na and decreasing Ca (Li et al. 2013a).

Hydrogeochemical Processes in the Zhiluo Group Aquifer

The Zhiluo Group, the main aquifer in the study area, is not only the main water supply source in the Ningtiaota Coalfield, but also the potential threat to coal mining because it overlies the coal-bearing Yan'an Group. Therefore, studies of hydrochemistry, flow paths, and hydraulic connection are vital. An insight into the hydrogeochemical processes can provide a basis for such studies. Dissolved species and their relationships can reveal the origin of chemical compositions and the hydrochemical processes that have generated the observed water compositions (Fisher and Mullican 1997). Groundwater generated under different causes or conditions have obvious differences in ion ratios, so ion ratios are used to determine sources or the evolution process of groundwater (Wu et al. 2014; Shen et al. 1986).

The correlation between two components or one component and several components can be expressed as scatter plots (Shen et al. 1986). Figure 8a, b presents the relationship between TDS and major ions concentrations. It shows that Ca and HCO_3 make the greatest contribution to TDS, followed by SO_4, Na, and Mg. With TDS growth, HCO_3, Ca, and Mg increase, while Na increases erratically, suggesting that the sources of Ca, Mg, and HCO_3 are relatively stable while the Na source is more complex. These relationships will be further discussed below.

Almost all of the water samples were in equilibrium/supersaturated with respect to calcite and dolomite (Table 1; Fig. 8d). Nevertheless, the saturation index (SI) of gypsum was below zero for all samples and tended to approach zero with increasing TDS, suggesting that gypsum dissolves along flow paths. Four samples (J13, J10, J11, and J15) plotted near the 1:1 line (Fig. 8f), which may indicate gypsum dissolution. However, gypsum dissolution may not be the primary source of Ca for most of

Table 2 Statistics of chemical compositions of the water samples; unit: mg/L

Types	Statistics	Ca	Mg	Na	K	HCO_3	SO_4	Cl	CO_3	NO_3	F	TDS
Surface water	Minimum	50.89	7.66	7.83	0.55	198.96	11.45	5.17	0.00	6.33	0.25	193.25
	Maximum	58.16	11.08	16.65	1.56	233.82	30.86	9.44	0.00	9.93	0.46	237.99
	Mean	54.67	9.33	11.25	1.06	214.32	17.96	6.65	0.00	8.08	0.32	216.49
Q_4^{eol} groundwater	Minimum	18.26	6.96	10.25	0.52	117.05	2.71	4.89	0.00	0.27	0.16	110.83
	Maximum	90.20	8.37	14.20	2.07	210.50	48.00	12.40	0.00	65.50	0.29	344.47
	Mean	51.75	7.66	11.34	1.21	167.21	26.13	7.38	0.00	26.52	0.23	215.86
J_2z groundwater	Minimum	1.68	0.16	6.60	0.50	14.46	2.40	3.08	0.00	0.00	0.08	77.84
	Maximum	49.10	15.80	53.90	16.16	204.40	60.00	24.80	21.34	19.80	1.85	258.37
	Mean	25.75	7.92	16.65	2.39	126.84	15.74	6.38	2.18	6.75	0.36	146.45
J_2y groundwater	Minimum	9.63	4.82	10.20	1.44	73.03	2.04	5.02	0.00	0.20	0.21	77.26
	Maximum	41.67	7.20	12.26	2.63	174.27	13.76	12.93	0.00	6.50	0.49	175.21
	Mean	25.83	6.01	11.47	1.80	124.53	9.08	8.69	0.00	2.77	0.32	128.21

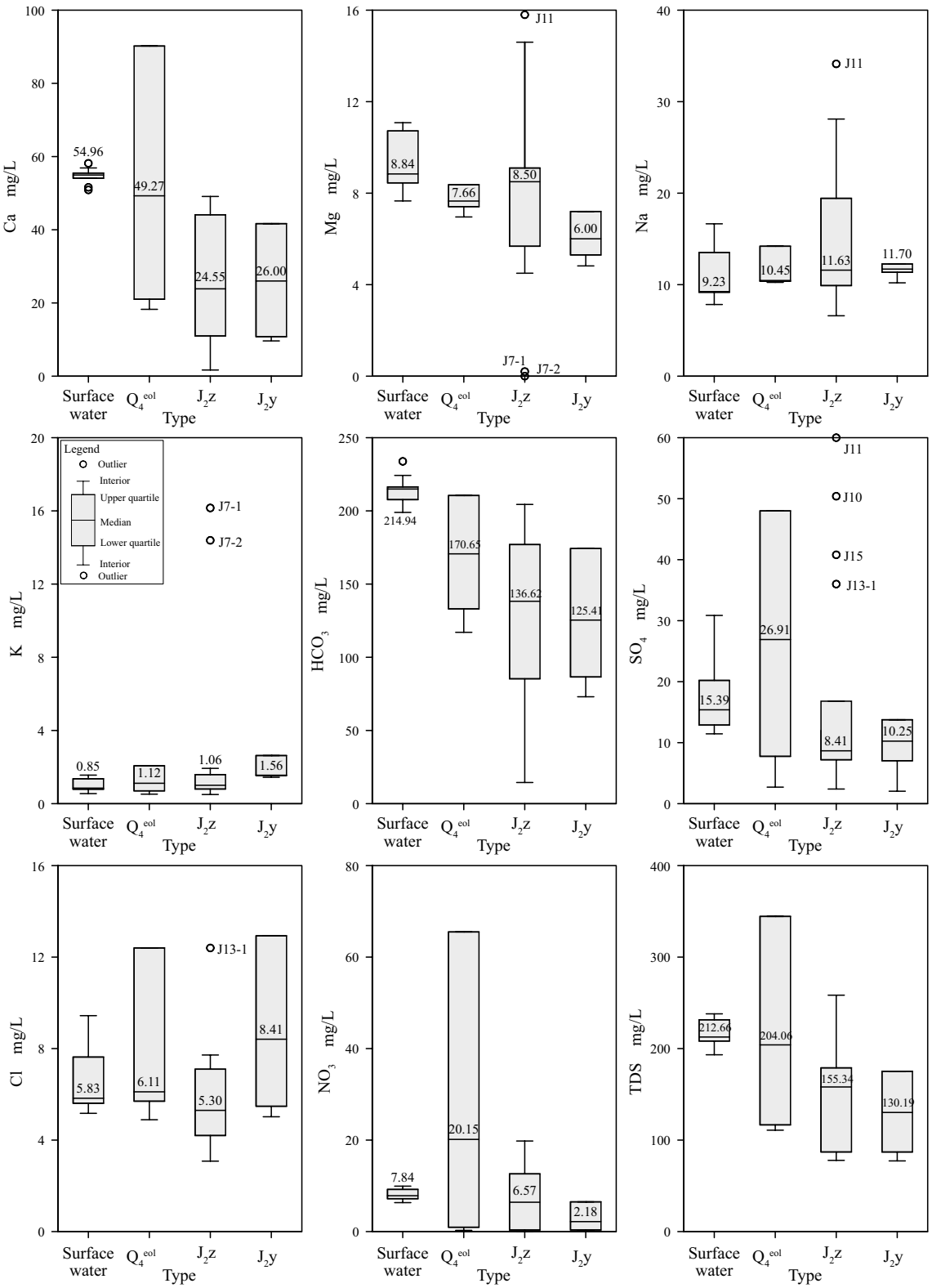

Fig. 4 Box-plots of groundwater chemical compositions

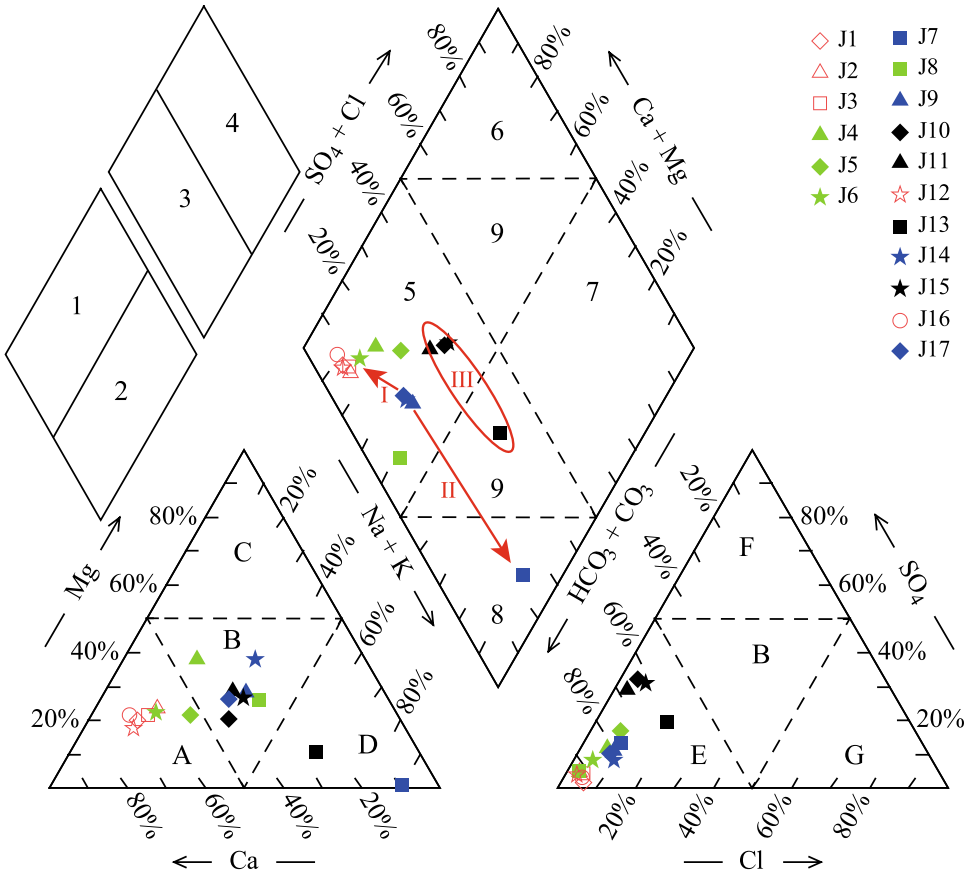

Fig. 5 Piper diagram of J_2z groundwater samples in the area: *1* alkaline earth exceeding alkalies; *2* alkalies exceeding alkaline earth; *3* weak acids exceeding strong acids; *4* strong acids exceeding weak acids; *5* carbonate hardness exceeds 50%; *6* non-carbonate hardness exceeds 50%; *7* alkalies and strong acids predominated; *8* alkaline earth and weak acids predominated; *9* mixed type; *A* calcium type; *B* no dominant type; *C* magnesium type; *D* sodium and potassium type; *E* bicarbonate type; *F* sulphate type; *G* chloride type

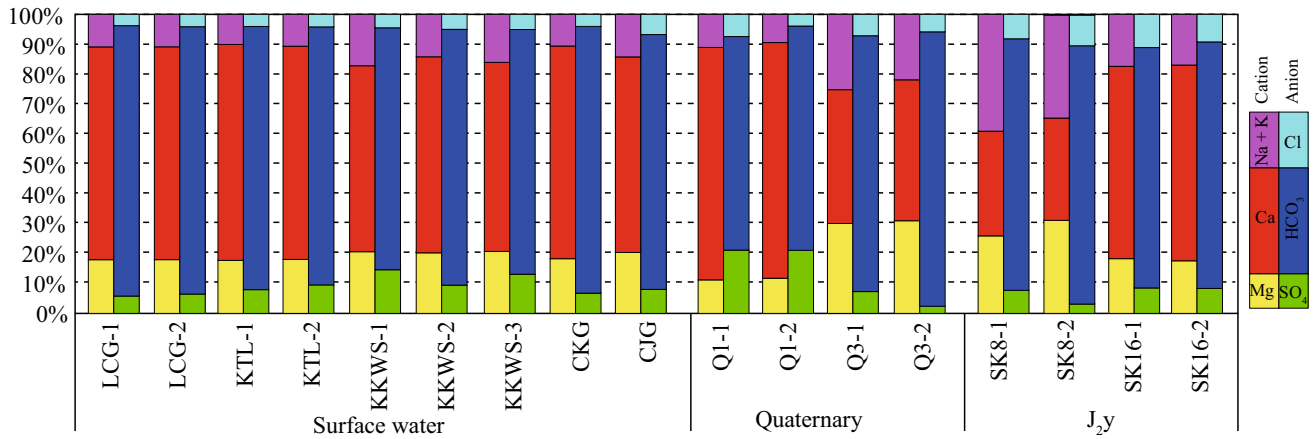

Fig. 6 Percentage histograms of water samples in the area

the samples; their ratios of Ca to SO_4 is far greater than 1 (Fig. 8f) and the correlation between SI_{gypsum} and Ca concentration is slightly weaker than that with SO_4 (Fig. 8e).

Among the major processes affecting alkalinity in aquatic systems (e.g. dissolution of minerals, sulfide oxidation/reduction), only silicate and carbonate dissolution increases alkalinity and Σ cations at the same time with nearly a 1:1 ratio (Kim 2003; Kim et al. 2005). The correction was made by subtracting (Cl) from the sum of the major cations (Σ Cation (meq/L) = Ca + Mg + Na + K − Cl), eliminating the possible influence of NaCl or $CaCl_2$ because dissolution of these salts doesn't affect alkalinity (Garrels and Mackenzie 1967).

The Zhiluo Group aquifer is characterized as a medium-coarse grained gravel-bearing feldspar sandstone, where silicates are the dominant minerals. The groundwater

is saturated/supersaturated with calcite and dolomite (Fig. 8d). Therefore, the approximately 1:1 increase in Σ cations and alkalinity (Fig. 8g) of the Zhiluo Group groundwater suggests dissolution of silicate minerals, especially plagioclase (Kim 2003). However, points that lie on the 1:1 line and above may indicate that gypsum dissolution also took place, leading to increased Ca without an increase in alkalinity.

The Σ cations and Cl or SO_4 produced by dissolution of chloride (NaCl and $CaCl_2$, etc.) and sulfate ($CaSO_4 \cdot 2H_2O$ etc.) salts are balanced in milliequivalents concentration, i.e. Σ cations/(Cl + SO_4) = 1. Since Cl-bearing and SO_4-bearing minerals are rare in the strata, the groundwater shows higher values of Σ cations/(Cl + SO_4) due to dissolution of silicate minerals (Fig. 8h). Human activities usually generate chloride salts (e.g. NaCl from salt, $CaCl_2$ from deicing salts) and sulfate salts (e.g. $MgSO_4$ and K_2SO_4 from fertilizers, $CaSO_4$ from cement materials; Kim et al. 2005) except for natural chloride and sulfate salts. Therefore, the Σ cations/(Cl + SO_4) would be close to 1 under intensive human activities. The high values of Σ cations/(Cl + SO_4) in Fig. 8h also indicate little influence of human activity on groundwater quality in the Zhiluo Group aquifer.

The value of (Na + K)/Cl about 1 indicates that the main source of Na and K is the dissolution of halite and sylvite (Shen et al. 1986). The value of (Na + K)/Cl above 1 reflects a contribution from silicate weathering by the release of Na and/or K apart from dissolution of halite and sylvite, or from the secondary processes, such as ion exchange between Ca and Na or K (Appelo and Postma 2005; Edmunds et al. 2003; Meybeck 1987). Thus, the value of (Na + K)/Cl can reflect a major source of Na and K in groundwater.

The (Na + K)/Cl values of the Zhiluo Group groundwater range from 2.13 to 13.68, with an average value of 4.91. Figure 8i shows that the points plot far above the 1:1 line, i.e., (Na + K)/Cl >> 1, suggesting that much of the alkalies in the analyzed groundwater samples may originate from weathering of silicate minerals rather than dissolution of halite and sylvite (Ghrefat et al. 2013). Meanwhile, cation exchange, which decreases the Ca content and increases the Na and/or K contents, is likely (Appelo and Postma 2005; Edmunds et al. 2003).

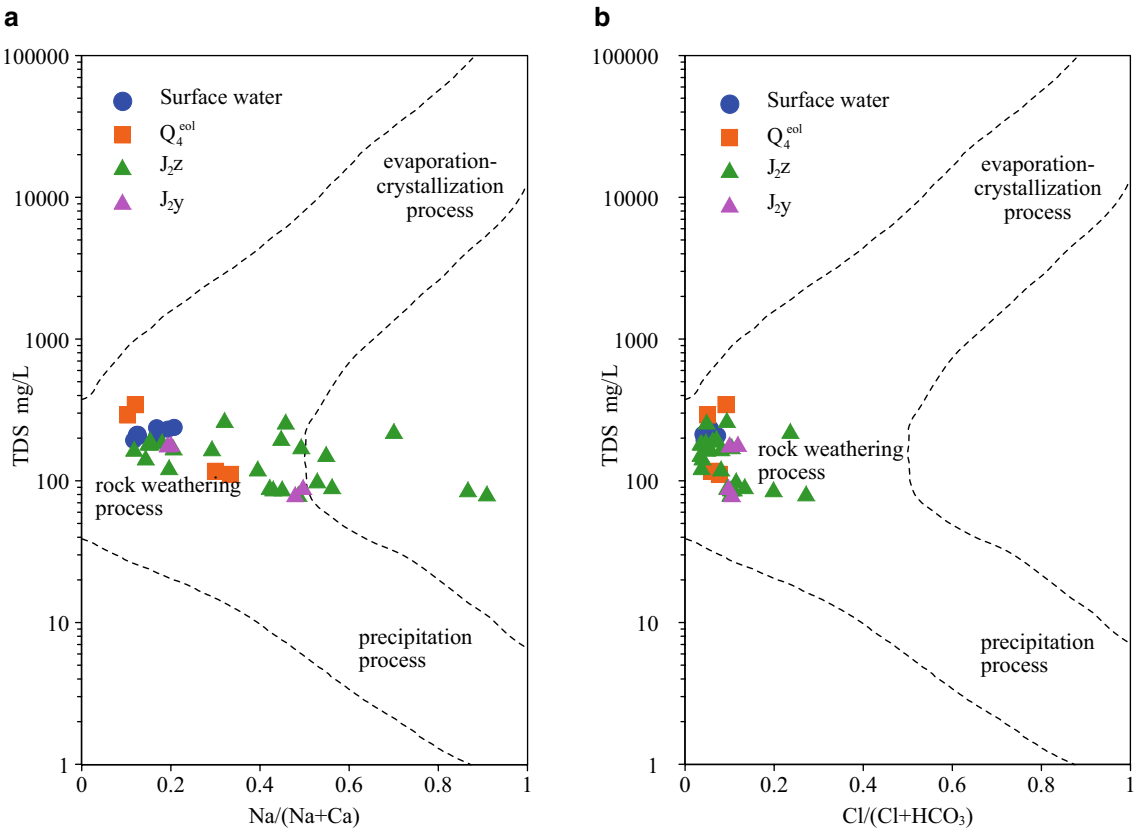

Fig. 7 Diagrammetic representation of processes controlling the chemistry of water samples in the area: **a** TDS vs gNa/g(Na + Ca), **b** TDS vs gCl/g(Cl + HCO_3)

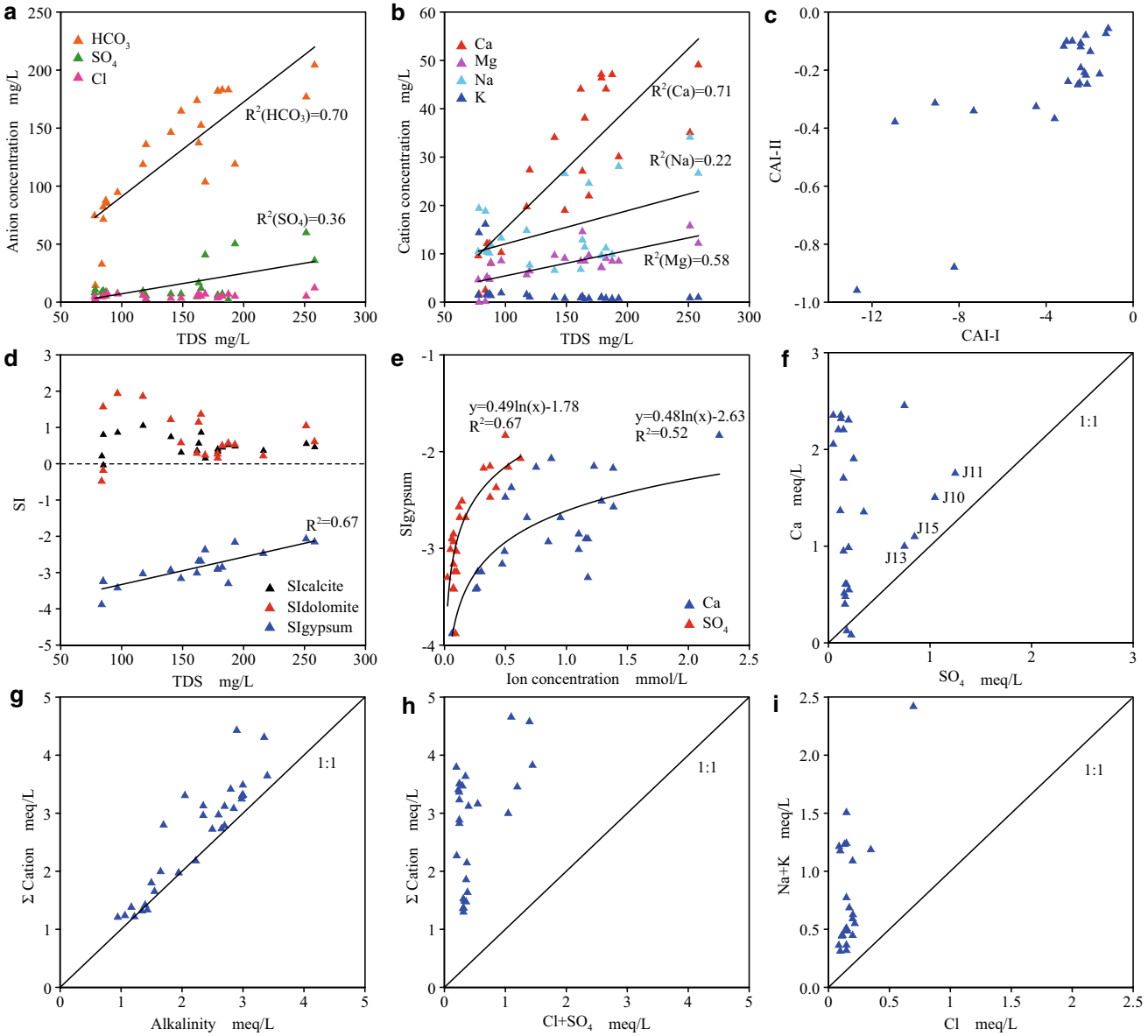

Fig. 8 Relationship between hydrochemical composiitions of Zhiluo Group groundwater: **a** TDS versus anions concentration, **b** TDS versus cations concentration, **c** the Schoeller indices, **d** equilibrium of groundwater with calcite, dolomite and gypsum, **e** SIgypsum versus concentration of Ca and SO_4, **f** ratios between Ca and SO_4, **g** relationship between corrected Σ Cation and alkalinity, **h** relations between Σ Cation and Cl + SO_4, **i** ratios between (Na + K) and Cl

Cation exchange can be studied through the chlor-alkaline indices proposed by Schoeller (Li et al. 2013b; Marghade et al. 2012). These Schoeller indices, such as CAI-I and CAI-II, are calculated by the following formulas (ion concentration in units of meq/L):

$$\text{CAI-I} = \frac{\text{Cl}^- - (\text{Na}^+ + \text{K}^+)}{\text{Cl}^-}, \tag{4}$$

$$\text{CAI-II} = \frac{\text{Cl}^- - \left(\text{Na}^+ + \text{K}^+\right)}{\text{HCO}_3^- + \text{SO}_4^{2-} + \text{CO}_3^{2-} + \text{NO}_3^-}. \tag{5}$$

If negative values for the Schoeller indices are obtained, Ca and/or Mg have been removed from solution, and Na and/or K have taken their place. If the indices are positive, then the inverse reactions have taken place (Li et al. 2013a). In the study area, all samples of Zhiluo Group groundwater had negative Schoeller indices values (Fig. 8c), indicating that Na and/or K in aquifer minerals have replaced Ca/Mg in groundwater (Eq. 3). This is consistent with the Gibbs diagram and (Na + K)/Cl ratio.

Stable Hydrogen and Oxygen Isotopes

The composition of stable hydrogen and oxygen isotopes is affected by meteorological processes. The values and distribution characteristics of δD and $\delta^{18}O$ provide a basis for the investigation of groundwater recharge sources. Craig (1961) first found a linear relationship between δD and $\delta^{18}O$ of global rainfall, namely the Craig equation, $\delta D = 8\delta^{18}O + 10$, which is called the global meteoric water line (GMWL) when plotted on the δD–$\delta^{18}O$ diagram (Zhou et al. 2010).

The local meteoric water lines (LMWL; $\delta D = 7.33\delta^{18}O + 2.14$) was obtained by Wang et al. (2010), using meteoric water data in the Yushenfu Coalfield from June to October in 2009, with δD values from −90.50 to −33.00‰, $\delta^{18}O$ values from −12.65 to −5.40‰, and deuterium excess parameters from 5 to 12‰. The study area is part of the Yushenfu Coalfield and so it seems to be reasonable to use the line as the LMWL of the study area. Figure 9 shows the relationship between δD and $\delta^{18}O$ in the study area. The points fall near the LMWL and below it, which indicates a meteoric origin accompanied by weak evaporation (Asmael et al. 2015; Gattacceca et al. 2009). The linear regression equation $\delta D = 6.09\delta^{18}O - 12.59$ ($R^2 = 0.87$) and LMWL intersect at point A (dδ = −86.36‰, $\delta^{18}O$ = −12.07‰), which reflects the average isotope composition of precipitation.

The two points plotting further to the right of the LMWL were respectively sampled from the CJG reservoir (−8.00, −61.83) and LCG River (−8.00, −60.33), which indicates more intense evaporation. The other surface water samples collected from rivers present isotopic compositions similar to groundwater samples. A previous study showed that groundwater discharge is one of the main sources of the LCG River especially during the dry seasons (Xi'an Research Institute 2012), so the above isotopic similarities may indicate that the sampled rivers were recharged by groundwater. The groundwater experienced weak evaporation which might have occurred during rainfall infiltration. The most depleted values of δD and $\delta^{18}O$ were measured in the water samples from borehole J7, which are at the left bottom of the figure, indicating that groundwater collected in J7 experienced the least evaporation of the groundwater sampled in the area. The zoom area of Fig. 8 shows that water samples collected from Q1 and J14 plotted relatively far away, although the two boreholes are only ten m away in the field. The same can be seen in the Q3 and J17 boreholes. These cases indirectly testify to the weak hydraulic connection between the Quaternary and Jurassic aquifers.

All samples were affected by evaporation to varying degrees, and the relationship between $\delta^{18}O$ and TDS can be analyzed to study the contribution of evaporation to the increase of TDS. A study carried by Clark and Fritz (1997) shows that the $\delta^{18}O$ values will increase by 25‰ when the water is concentrated five times (TDS increases fivefold) at a humidity of 50%. In the present study, although the TDS increased about five times (from 70 to 350 mg/L), the $\delta^{18}O$ values ranged between −10 and −8‰, with a range of only 2‰ (Fig. 10), which indicates that evaporation contributed little to the increase of TDS. The relation between $\delta^{18}O$ and TDS further supports the hypothesis that the regional groundwater is not strongly affected by evaporations, and that rock weathering controls the TDS, in accordance with the previously discussed Gibbs diagrams.

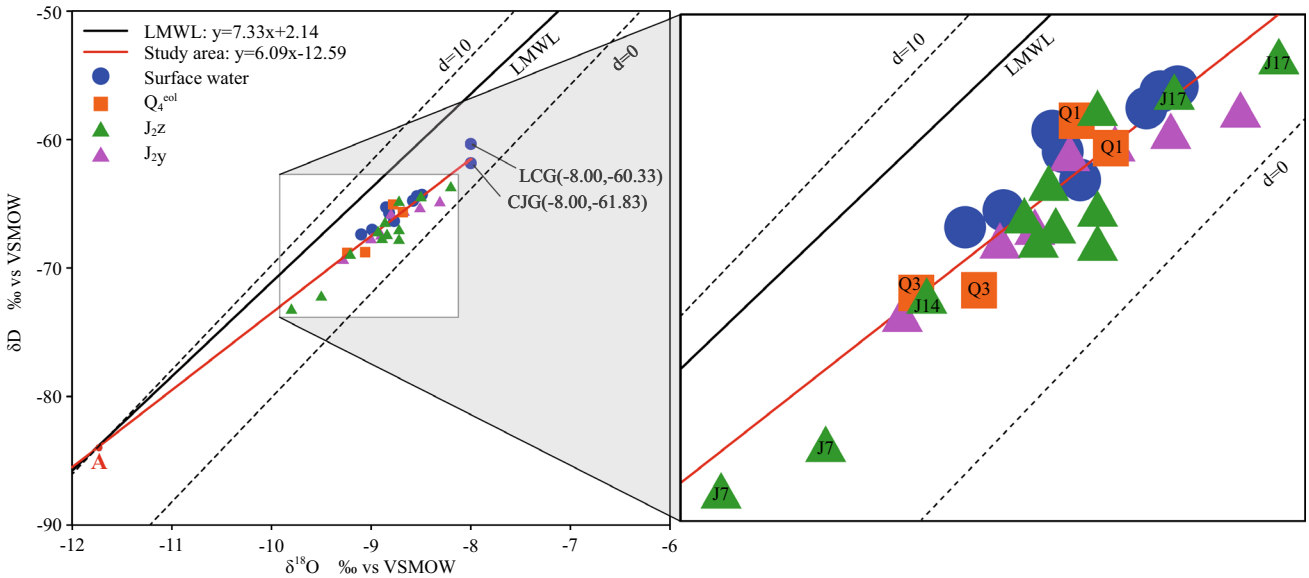

Fig. 9 Relationship between δD and $\delta^{18}O$ in the study area

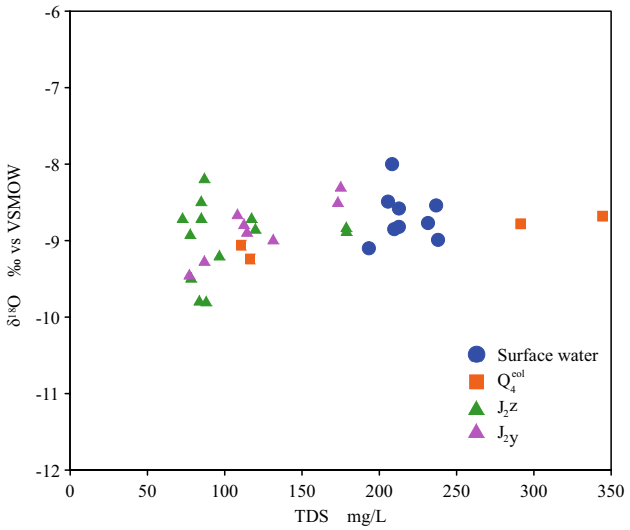

Fig. 10 Ranges of $\delta^{18}O$ and TDS in the study area

Conclusions

Similar to many coal mines in northwestern China, long-term pumping of groundwater has increased competition between groundwater resource protection and mine safety in the Ningtiaota Coalfield. Therefore, study of groundwater behavior and associated hydrodynamic and hydrochemical processes have become key aspects for sustainable development of the area.

Concentrations of major ions were low in both surface water and groundwater, although the surface water tended to have slightly higher concentrations of dissolved ions. The sampled water had a low salinity (TDS < 500 mg/L) and very soft (0–75 mg/L) to medium hard (150–300 mg/L) hardness, and all of the samples were dominantly of the HCO_3–Ca type. The Zhiluo Group groundwater was determined to be of good quality, with little evidence of pollution by anthropogenic activities, making it is fit for water supply of any purpose. High NO_3 concentrations were detected in the Quaternary groundwater, which indicates the significant impact of agricultural activities on the shallow Quaternary groundwater.

The main water–rock interactions controlling the groundwater chemistry of the Zhiluo Group are the precipitation of calcite and dolomite, dissolution of silicate minerals (especially plagioclase) and gypsum, and cation exchange, which increased SO_4^{2-} concentrations locally. The hydrochemistry of the Zhiluo Group was dominated by natural geochemical processes, without much influence by coal mining, perhaps because the water was sampled when mining in the coalfield was still at its initial stage. Continued monitoring is suggested to identify any possible water quality changes that may occur due to the subsequent mining activities.

The stable isotopes reveal that the surface water and groundwater in the study area originated from atmospheric precipitation and had not been strongly affected by evaporation. The elevated TDS appears to be mainly due to weathering of rock-forming minerals, which would be consistent with the hydrochemical results. It can be deduced from drainage tests and isotopic characteristics that there is a weak hydraulic connection between the Quaternary and Jurassic aquifers. The results of this study may be useful to water resources management and groundwater inrush prevention in the coalfield and other coal mines.

Acknowledgements This work was supported by the National Natural Science Foundation of China under Grants 41272269 and 41672243. We thank Dr. Xiang Ding, Shao Hongqi, Han Qiang, Wang Xiaoming, Xie Guilin, and other staff from CCTEG Xi'an Research Institute and the Ningtiaota Coal Mining Administration for their assistance in field work. We gratefully acknowledge comments and helpful information from the editors and the four anonymous reviewers.

References

André L, Franceschi M, Pouchan P, Atteia O (2005) Using geochemical data and modelling to enhance the understanding of groundwater flow in a regional deep aquifer, Aquitaine Basin, southwest of France. J Hydrol 305(1–4):40–62

Appelo CAJ, Postma D (2005) Geochemistry, groundwater and pollution. A. A. Balkema Publishers, Leiden

Asmael NM, Huneau F, Garel E, Celle-Jeanton H, Le Coustumer P, Dupuy A, Hamid S (2015) Origin and recharge mechanisms of groundwater in the upper part of the Awaj River (Syria) based on hydrochemistry and environmental isotope techniques. Arab J Geosci 8(12):10521–10542

CCTEG (China Coal Technology & Engineering Group) Xi'an Research Institute (2012) The comprehensive hydrogeological reports of Ningtiaota Minefield. CCTEG Xi'an Research Institute, Xi'an **(in Chinese)**

Chen LW, Yin XX, Liu X (2013) Tracing of recharge sources of deep aquifers in the concealed type colliery of North China by hydrochemistry and isotopes. Sci Geogr Sinica 33(6):755–762

Clark ID, Fritz P (1997) Environmental isotopes in hydrogeology. Lewis, Boca Raton

Craig H (1961) Isotopic variations in meteoric waters. Science 133(3465):1702–1703

Ding WL, Dai P, Zhu DW, Zhang YQ, He JH, Li A, Wang RY (2016) Fractures in continental shale reservoirs: a case study of the Upper Triassic strata in the SE Ordos Basin, Central China. Geol Mag 153(4):663–680

Edmunds WM, Guendouz AH, Mamou A, Moulla A, Shand P, Zouari K (2003) Groundwater evolution in the Continental Intercalaire aquifer of southern Algeria and Tunisia: trace element and isotopic indicators. Appl Geochem 18(6):805–822

Fisher RS, Mullican WF III (1997) Hydrochemical evolution of sodium-sulfate and sodium-chloride groundwater beneath the Northern Chihuahuan Desert, Trans-Pecos, Texas, USA. Hydrogeol J 5(2):4–16

Garrels RM, Mackenzie FT (1967) Origin of the chemical compositions of some springs and lakes. Adv Chem 67(10):222–242

Gastmans D, Chang HK, Hutcheon I (2010) Groundwater geochemical evolution in the northern portion of the Guarani Aquifer System (Brazil) and its relationship to diagenetic features. Appl Geochem 25(1):16–33

Gattacceca JC, Vallet-Coulomb C, Mayer A, Claude C, Radakovitch O, Conchetto E, Hamelin B (2009) Isotopic and geochemical characterization of salinization in the shallow aquifers of a reclaimed subsiding zone: the southern Venice Lagoon coastland. J Hydrol 378(1–2):46–61

Ghrefat HA, Batayneh A, Zaman H, Zumlot T, Elawadi E, Nazzal Y (2013) Major ion chemistry and weathering processes in the Midyan Basin, northwestern Saudi Arabia. Environ Monit Assess 185(10):8695–8705

Gibbs RJ (1970) Mechanisms controlling world water chemistry. Science 170(3962):1088–1090

Gomo M, Vermeulen D (2014) Hydrogeochemical characteristics of a flooded underground coal mine groundwater system. J Afr Earth Sci 92:68–75

Han Y, Wang GC, Cravotta CA, Hu WY, Bian YY, Zhang ZW, Liu YY (2013) Hydrogeochemical evolution of Ordovician limestone groundwater in Yanzhou, North China. Hydrol Process 27(16):2247–2257

Hu W, Evans R (1997) The impacts of coal mining in Shenmu County, the Loess Plateau, China. Ambio 26(6):405–406

Huang PH, Chen JS (2012) Recharge sources and hydrogeochemical evolution of groundwater in the coal-mining district of Jiaozuo, China. Hydrogeol J 20(4):739–754

Jiang XH, Gu XW, He HM (2010) The influence of coal mining on water resources in the Kuye River Basin. J Nat Resour 25(2):300–306 **(in Chinese)**

Kendall C, McDonnell JJ (1998) Isotope tracers in catchment hydrology. Elsevier, Amsterdam

Kim K (2003) Long-term disturbance of ground water chemistry following well installation. Ground Water 41(6):780–789

Kim K, Rajmohan N, Kim HJ, Kim SH, Hwang GS, Yun ST, Gu B, Cho MJ, Lee SH (2005) Evaluation of geochemical processes affecting groundwater chemistry based on mass balance approach: a case study in Namwon, Korea. Geochem J 39(4):357–369

Li PY (2016) Groundwater quality in western China: challenges and paths forward for groundwater quality research in western China. Expos Health (London) 8(3):305–310

Li ZX, Han ML, Li JT, Yu JF, Lü DW, Liu HF (2008) On the analysis of the high-resolution sequence stratigraphy and coal accumulating law of jurassic in Ordos Basin. J Coal Sci Eng 14(1):85–91

Li PY, Qian H, Wu JH, Zhang YQ, Zhang HB (2013a) Major ion chemistry of shallow groundwater in the Dongsheng coalfield, Ordos Basin, China. Mine Water Environ 32(3):195–206

Li PY, Wu JH, Qian H (2013b) Assessment of groundwater quality for irrigation purposes and identification of hydrogeochemical evolution mechanisms in Pengyang County, China. Environ Earth Sci 69(7):2211–2225

Li PY, Qian H, Howard KWF, Wu JH (2015) Building a new and sustainable "Silk Road economic belt". Environ Earth Sci 74(10):7267–7270

Marghade D, Malpe DB, Zade AB (2012) Major ion chemistry of shallow groundwater of a fast growing city of Central India. Environ Monit Assess 184(4):2405–2418

Meybeck M (1987) Global chemical-weathering of surficial rocks estimated from river dissolved loads. Am J Sci 287(5):401–428

Ministry of Land and Resources of the People's Republic of China (1993) Quality standard for ground water vol GB/T 14848–93. Standard Press of China, Beijing

Monjerezi M, Vogt RD, Aagaard P, Saka JDK (2011) Hydro-geochemical processes in an area with saline groundwater in lower Shire River valley, Malawi: an integrated application of hierarchical cluster and principal component analyses. Appl Geochem 26(8):1399–1413

Moral F, Cruz-Sanjulian JJ, Olias M (2008) Geochemical evolution of groundwater in the carbonate aquifers of Sierra de Segura (Betic Cordillera, southern Spain). J Hydrol 360(1–4):281–296

Murkute YA (2014) Hydrogeochemical characterization and quality assessment of groundwater around Umrer coal mine area Nagpur District, Maharashtra, India. Environ Earth Sci 72(10):4059–4073

Piper AM (1944) A graphic procedure in the geochemical interpretation of water-analyses. Eos Trans AGU 25(6):914–928

Shaanxi Coalfield Geology Bureau (1987) The detailed geology reports of coal mines in Shenmu. Shaanxi Coalfield Geology Bureau, Shaanxi **(in Chinese)**

Shen ZL, Zhu WH, Zhong ZS (1986) Fundamental hydrogeochemistry. Geological Publishing House, Beijing **(in Chinese)**

Shvartsev SL, Wang YX (2006) Geochemistry of sodic waters in the Datong intermountain basin, Shanxi Province, Northwestern China. Geochem Int 44(10):1015–1026

Su H, Kang WD, Cao ZZ, Zhu HL (2013) Analysis on precipitation and runoff changing trend from 1954 to 2009 in Kuye River Basin. Ground Water 35(6):14–17 **(in Chinese)**

Subrahmanyam K, Yadaiah P (2001) Assessment of the impact of industrial effluents on water quality in Patancheru and environs, Medak district, Andhra Pradesh, India. Hydrogeol J 9(3):297–312

Sun FQ, Hou GC, Dou Y, Fang CS, Jiang J, Zhang LZ (2009) Hydrogeochemistry evidence of groundwater circulation features in Ordos Cretaceous basin—a case study in Chabu well field. J Jilin U Earth Sci 39(2):269–275+293 **(in Chinese)**

Wang GC, Duan Q, Chang YS (2000) Hydro-geochemical exploratory method in mine groundwater hazard control. Chin J Geol Hazard Control 11(1):36–40+43 **(in Chinese)**

Wang YX, Guo QH, Su CL, Ma T (2006) Strontium isotope characterization and major ion geochemistry of karst water flow, Shentou, northern China. J Hydrol 328(3–4):592–603

Wang SM, Fan LM, Huang QX, Yang ZY, Wang GZ, Shen T (2009) Study on coal mining for protecting ecological water level in the ecological fragile mining area. Metal Mine A1:715–720+725 **(in Chinese)**

Wang L, Wei SP, Zhang QF, Wang QJ, Li SQ (2010) Isotopic characteristics of water within the soil–vegetation–atmosphere system in the Yushenfu mining area. J Chin Coal Soc 35(8):1347–1353 **(in Chinese)**

Wang P, Yu JJ, Zhang YC, Liu CM (2013) Groundwater recharge and hydrogeochemical evolution in the Ejina basin, northwest China. J Hydrol 476:72–86

Wang XM, Jiao YQ, Wu LQ, Rong H, Wang XM, Song J (2014) Rare earth element geochemistry and fractionation in Jurassic coal from Dongsheng-Shenmu area, Ordos Basin. Fuel 136:233–239

Wu JH, Li PY, Qian H, Duan Z, Zhang XD (2014) Using correlation and multivariate statistical analysis to identify hydrogeochemical processes affecting the major ion chemistry of waters: a case study in Laoheba phosphorite mine in Sichuan, China. Arab J Geosci 7(10):3973–3982

Xue CJ, Chi GX, Xue W (2010) Interaction of two fluid systems in the formation of sandstone-hosted uranium deposits in the Ordos Basin: geochemical evidence and hydrodynamic modeling. J Geochem Explor 106(1–3):226–235

Yang H, Liu X, Yan X, Zhang H (2015a) Discovery and reservoir-forming geological characteristics of the Shenmu Gas Field in the Ordos Basin. Nat Gas Ind B 2(4):295–306

Yang MH, Li L, Zhou J, Jia HC, Sun X, Gong T, Ding C (2015b) Structural evolution and hydrocarbon potential of the upper Paleozoic Northern Ordos Basin, North China. Acta Geol Sin Engl 89(5):1636–1648

Yao JM, Xia F (2007) A study on hydrogeological condition and mining method in Ningtiaota Minefield (south limb), Shenmu-Fugu mining area. Coal Geol China 19(1):33–35+59 **(in Chinese)**

Zhang FE, Liu WS (2002) A Numerical Simulation on the Influence of underground water flow regime caused by coal mining—a case study in Daliuta, Shenfu Ming area. J Safe Environ 2(4):30–33 **(in Chinese)**

Zhou X, Jin XM, Liang SH, Shen Y, Zhang HM (2010) Specialized groundwater sciences. Geological Publishing House, Beijing **(in Chinese)**